Eddy-Current Displacement Transducer With Extended Linear Range and Automatic Tuning

Darko Vyroubal, *Member, IEEE*

***Abstract*—Design details and measurement results of the eddy-current displacement transducer with extended linear range and automatic tuning are presented. The transducer is based on a resonant impedance inversion method of transfer curve linearization where the displacement probe circuit is kept in resonance by the resonance control loop. The transducer exhibits an extended linear range due to the compensation of displacement probe losses by a negative impedance converter (NIC) at the transducer input. Particular attention is paid to the NIC design and its temperature compensation. The new voltage-controlled NIC circuit is introduced, which can easily be realized with a standard commercial integrated circuit (LM 1496). Details of the transducer's reference generator and the NIC control voltage generator are also presented. The transducer's linear range extends from 0.25 to 3.75 mm (approximately 44% of the 8-mm probe diameter) while maintaining nonlinearity within $\pm 2\%$ F.S. This result is, at least, a 75% improvement to the best commercially available eddy-current displacement transducers (a linear range of 80 mil $\sim$ 2 mm for an 8-mm probe). Further linearization can be achieved by postlinearization of the detected signal.**

***Index Terms*—Automatic resonance tuning, contactless displacement transducer, eddy currents, linear-range extension, negative impedance converter (NIC), probe losses compensation, resonant impedance inversion.**

I. Introduction

THE BLOCK diagram of the eddy-current displacement transducer with extended linear range and automatic tuning is depicted in Fig. 1. The initial design of this transducer was introduced in [1] but without the probe losses compensation, e.g., no extension of the linear range was attempted. The detailed analysis of the transducer performance was also not presented in [1]. The transducer consists of a probe and a signal-processing unit connected to the probe via a coaxial extension cable. The probe is a simple usually coreless coil that is placed at the tip of a suitable probe body. The purpose of the signal-processing unit is to excite the probe with a high frequency current (1 MHz) and to detect the voltage that was developed across the parallel tank circuit with the probe impedance (lossy inductance) and the total parallel capacitance with the cable capacitance and the transducer input capacitance. The detected voltage is resolved into the in-phase I and quadrature Q components. The in-phase component is proportional to the probe-to-target displacement and is used for displacement transducing, whereas the quadrature component is proportional to the resonance detuning and is used by the automatic resonance control loop to keep the tank in resonance. The physical basis of probe-to-target displacement transducing and the probe mathematical model are described in more detail in [2].

Manuscript received February 13, 2008; revised May 16, 2008. Current version published August 12, 2009. The Associate Editor coordinating the review process for this paper was Dr. Subhas Mukhopadhyay.

The author is with the Polytechnic University of Karlovac, 47000 Karlovac, Croatia (e-mail: darko.vyroubal@vuka.hr).

Digital Object Identifier 10.1109/TIM.2009.2017165

II. Equivalent Input Circuit

The equivalent input circuit comprises the probe equivalent impedance $Z(d)$ in parallel to the total capacitance C and parallel to the total input resistance R. The probe-equivalent impedance model is developed in [2] as a series lossy tank circuit above the series (current) resonance, e.g., the reactance is inductive. The probe reactance and the probe series resistance (probe losses) are sensitive to probe-to-target displacement. The probe resistance is used for displacement transducing in the signal-processing unit. The total parallel capacitance consists of the cable capacitance C_{P} and the tuning capacitance C_{T}, with the preamplifier input capacitance in parallel to the capacitance of the tuning varicap diode. The preamplifier input capacitance is very low compared to the varicap capacitance; thus, it can usually be ignored. The total input resistance comprises a parallel connection of the negative resistance R_N of the negative impedance converter (NIC) and the equivalent input resistance R_i of the preamplifier in parallel to the excitation current generator. The equivalent input circuit diagram is shown in Fig. 2.

The probe impedance elements are given as follows [2].

- X_0 Probe intrinsic inductive reactance when not influenced by the eddy currents in the target, e.g., probe that is far from the target.
- $X_r(d)$ Probe reflective capacitive reactance, which is the result of eddy-current losses in the target and is displacement dependent.
- $X(d)$ Total probe inductive reactance, which is displacement dependent.
- R_0 Probe intrinsic series loss resistance when not influenced by the eddy currents in the target, e.g., probe that is far from the target.
- $R_r(d)$ Probe reflective series loss resistance, which is result of eddy-current losses in the target and is displacement dependent.
- $r(d)$ Total probe series loss resistance, which is displacement dependent.

The equivalent input circuit impedance can be expressed as

$$Z = \mathrm{Re}[Z] + j\mathrm{Im}[Z] = |Z| \cdot e^{j\varphi}. \tag{1}$$

The circuit is in resonance when the impedance phase angle is equal to zero, which makes φ the very parameter that was used by the resonance control loop as the error signal. It is

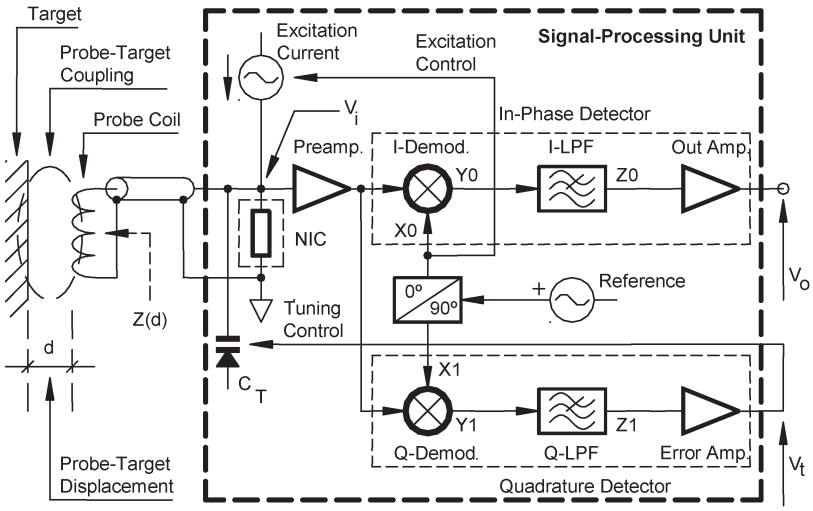

Fig. 1. Block diagram of the improved eddy-current displacement transducer with extended linear range and automatic tuning. It is based on the block diagram introduced in [1].

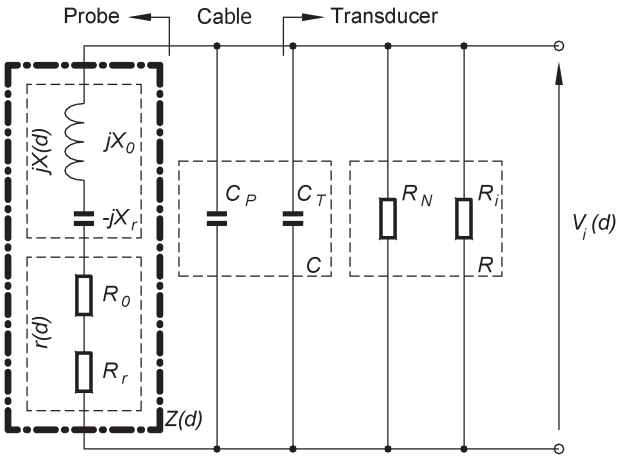

Fig. 2. Equivalent input circuit diagram.

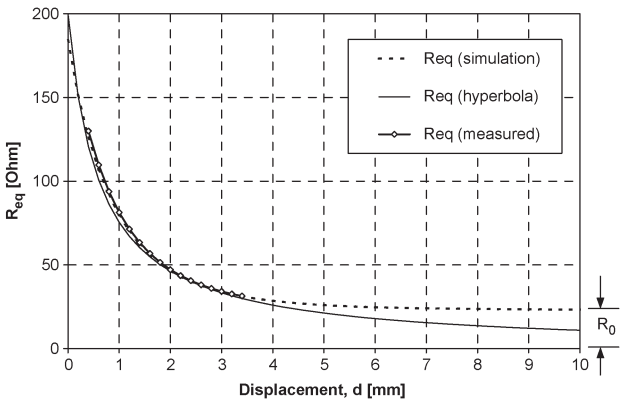

Fig. 3. Comparison of the measured [1] and simulated [2] total probe series loss resistance to the interpolated hyperbola.

reasonable to assume that the resonance control will exhibit a small residual error, e.g., residual φ. Considering φ as a detuning measure, one can resolve impedance in resonance by the inspection of the equivalent circuit, i.e.,

$$|Z(d)|_{\rm res} = \frac{r^2(d)+X^2(d)}{r(d)+\frac{r^2(d)+X^2(d)}{R}} \qquad R = R_N \parallel R_i \tag{2}$$

with the parallel capacitive reactance X_C being required for the resonance tuning, which is maintained by the resonance control loop. We have

$$X_C(d) = \frac{r^2(d)+X^2(d)}{X(d)-\left[r(d)+\frac{r^2(d)+X^2(d)}{R}\right]\cdot\tan\varphi}. \tag{3}$$

The real part of the impedance is then equal to

$$\mathrm{Re}\,[Z(d)] = \frac{|Z(d)|_{\rm res}}{1+\tan^2\varphi}. \tag{4}$$

In addition, the in-phase voltage that was developed across the tank is equal to the voltage drop on $\mathrm{Re}[Z(d)]$ that was produced by the excitation current.

III. Resonant Impedance Inversion

By the inspection of (2), it follows that $\mathrm{Re}[Z(d)]$ is displacement dependent through $r(d)$ and $X(d)$. The dependence of $r(d)$ and $X(d)$ on displacement was experimentally established in [1] and theoretically analyzed in [2]. The variation over the displacement range is about 10% for $X(d)$, whereas for $r(d)$, it is approximately 10:1. Thus, $r(d)$ is used for displacement transducing. Comparison of the measured [1] and the simulated [2] $r(d)$ (labeled $R_{\rm eq}$ as in [1] and [2]) to the interpolated hyperbola is shown in Fig. 3. Fig. 3 follows an almost-hyperbolic behavior of $r(d) \sim C/d$ over small to medium displacement range, whereas for large displacements, it is almost constant, which is masked by the probe intrinsic series loss resistance R_0. The total probe series loss resistance $r(d)$ can be modeled as a series connection of the probe reflective series loss resistance $R_r(d)$, which is almost hyperbolic [1], [2], and the constant probe intrinsic series loss resistance R_0. Introducing this model into (2) gives

$$|Z(d)|_{\rm res} = \frac{r^2(d)+X^2(d)}{R_r(d)+\left[R_0+\frac{r^2(d)+X^2(d)}{R}\right]} = \frac{A}{R_r(d)+B}. \tag{5}$$

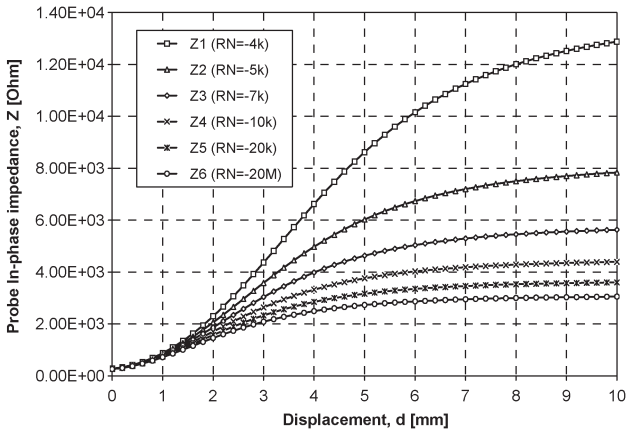

Fig. 4. Linearization of the transducer for various amounts of negative resistance added by the NIC.

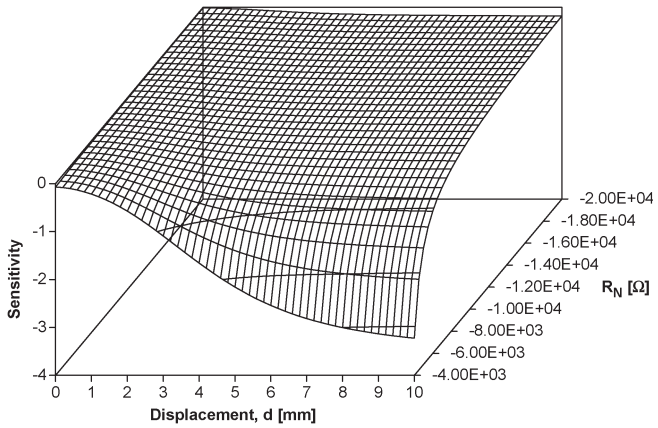

Fig. 5. Sensitivity of $|Z(d)|_{\rm res}$ to displacement d and negative resistance R_N.

$X(d)$ is only slightly dependent on d and is almost ten times bigger than $r(d)$ [1], [2]; thus, one can assume that A and B in (5) are almost constant with respect to d. On the other hand, R can be made negative by proper adjustment of R_N, canceling R_0 in B and making B in (5) vanish. Then, $|Z(d)|_{\rm res}$ becomes almost linear in d, i.e.,

$$|Z(d)|_{\rm res} \approx \frac{A}{R_r(d)} \approx \frac{A}{\frac{C}{d}} \approx D \cdot d \tag{6}$$

because $R_r(d)$ is almost hyperbolic with respect to d, $R_r(d) \approx C/d$, and the linearization of the transducer is achieved through resonant impedance inversion. The amount of negative resistance R_N that was added by the NIC is limited to keep the total resistance of the input circuit positive (otherwise, the transducer would turn into an oscillator). Simulation results for various values of R_N and $r(d)$ as in [2] and for $R_i = 10$ kΩ are shown in Fig. 4. The linear range for $R_N = -4$ kΩ is approximately 1.5–5.5 mm, whereas for $R_N = -20$ MΩ (almost no negative conductance applied), it is 0.5–2.5 mm. Application of the negative resistance has significantly extended the linear range. The side effect is the introduction of approximately 1 mm of additional linear-range offset from the probe tip, which can easily be accommodated for by displacing the probe coil for this amount deeper into the probe body.

IV. Sensitivity

The transducer transfer curve is dependent on the applied negative conductance (see Fig. 4) and on the performance of the resonance control, e.g., residual impedance phase error (4). Both aspects are prone to variation that was induced by several factors such as operating temperature, element tolerances, and aging. Sensitivities to R_N and φ are analyzed to establish transducer design constraints.

A. Sensitivity to R_N

Sensitivity to R_N follows after a partial differentiation of (2) in

$$S_{R_N}^{|Z(d)|_{\rm res}} = \frac{\frac{\partial |Z(d)|_{\rm res}}{|Z(d)|_{\rm res}}}{\frac{\partial R_N}{R_N}} = \frac{|Z(d)|_{\rm res}}{R_N} \tag{7}$$

with respect to R_N. Based on (7), it follows that the sensitivity is dependent on d. It is plausible, because for small to medium d, the probe losses are mainly caused by eddy currents in the target, whereas for large d, it is mainly caused by probe intrinsic losses and R_N. The sensitivity dependence on d and R_N is shown in Fig. 5. As expected, sensitivity is the highest for large d and maximum negative conductance applied. However, it is reasonably limited to approximately -3. Such sensitivity is not prohibitively high, making the transducer construction feasible by careful design.

B. Sensitivity to φ

Sensitivity to φ follows after a partial differentiation of (4) with respect to φ, i.e.,

$$S_{\varphi}^{{\rm Re}|Z(d)|} = \frac{\frac{\partial {\rm Re}|Z(d)|}{|Z(d)|}}{\frac{\partial \varphi}{\varphi}} = -2\varphi \cdot \tan\varphi. \tag{8}$$

Based on (8), it is evident that the sensitivity to resonance detuning could be quite large, because φ and $\tan\varphi$ rapidly rise with detuning if the tank quality factor Q_T is at least reasonably high $(Q_T > 10)$. Further assessment of sensitivity to resonance detuning requires analysis of the resonance control-loop performance.

V. Resonance Control Loop

The resonance control-loop model is derived based on Fig. 1 and the clarification of in-phase and quadrature detection process of the voltage across the tank as in Fig. 6. Detectors are simple switches followed by low-pass filters that extract dc voltages proportional to displacement and the residual phase error. The detected quadrature component Y_1 of V_i is low-pass filtered, which produces a dc voltage Z_1. We have

$$Z_1(d) = -\frac{V_i(d)}{\pi} \cdot \sin\varphi \tag{9}$$

which is in the error amplifier combined with amplifier offset and amplified to the tuning voltage level. We have

$$V_t(d) = K \cdot \left[V_{\rm os} - \frac{V_i(d)}{\pi} \cdot \sin\varphi \right] \tag{10}$$

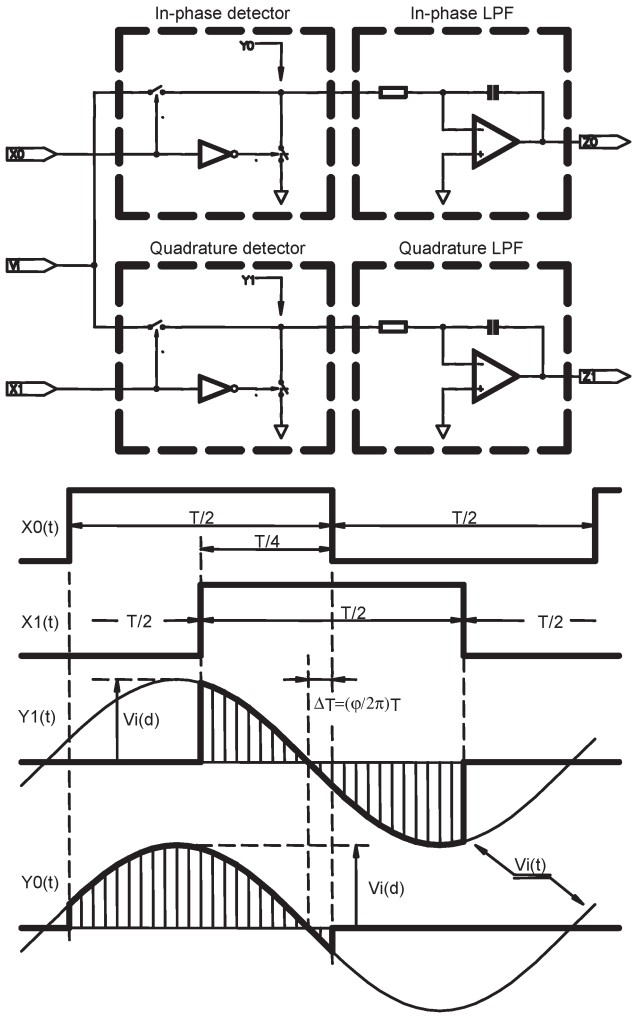

Fig. 6. In-phase and quadrature detection of the voltage at the input of the signal-processing unit.

where K is the amplifier gain, and $V_{\rm os}$ is the amplifier offset voltage. The varicap sensitivity to the tuning voltage is shown in (11) [3], where C_P is the tank parallel capacitance, and Q_p is the probe quality factor, with $Q_p(d) = X(d)/r(d)$ (not the total tank quality factor Q_T, although $Q_T \approx Q_P$ for low parallel loading, e.g., high R). We have

$$\frac{\Delta C_V(V_t)}{C_{VB}} = \frac{1}{\left(1 + \frac{1}{1-\frac{\Phi}{V_B}} \cdot \frac{V_t}{V_B}\right)^n} - 1 \qquad (11)$$

where C_{VB} is the varicap capacitance at the varicap bias voltage V_B, Φ is the p-n junction contact potential (≈0,7 V in Si), and n is the exponent that describes the varicap p-n junction type ($n = 1/2$ for an abrupt junction and $n = 1/3$ for a graded junction). $\Delta C_V(V_t)$ is the change of the varicap capacitance at the varicap bias voltage V_B relative to the control voltage $V_t - V_B$.

The tank impedance phase sensitivity to the varicap capacitance is evaluated by an analysis of the equivalent input circuit in Fig. 2. We have

$$\varphi(d) = \arctan\left[-Q_p(d) \cdot \frac{\frac{\Delta C_V(d)}{C_{VB}}}{1 + \frac{C_P}{C_{VB}}}\right] \qquad (12)$$

where $\Delta C_V = 0$, and the tank is assumed to be in resonance.

The control-loop equation is derived based on Fig. 1 by inspection. For a steady-state phase error, the loop equation reads

$$\varphi = \varphi\left(\frac{\Delta C_V(V_t)}{C_V}\right) - \varphi_0 \qquad (13)$$

where φ_0 is the initial resonance detuning phase error.

Combining (9)–(13), the resonance control-loop steady-state equation is derived as in (14), shown at the bottom of the page.

The resonance control-loop model based on (14) is shown in Fig. 7. Equation (14) is a trigonometric equation that was numerically solved for various combinations of initial tank resonant frequency detuning, error amplifier gain, and offset. The initial detuning phase error is proportional to the tank resonant frequency detuning and the probe quality factor Q_P, which is displacement dependent. We have

$$\varphi_0 = \arctan\left[-2 \cdot Q_P(d) \cdot \delta_\omega\right] \qquad \delta_\omega = \pm\frac{\Delta\omega_{\rm res}}{\omega_{\rm res}} \qquad (15)$$

where δ_ω is the relative resonant *frequency detuning* that was in solution to (14) and is assumed to be limited to ±10%. The total equivalent amplifier offset voltage was assumed to be within ±10 mV (which is rather conservative for modern operational amplifiers). The solution to (14) was sought for the minimum and maximum negative conductance of the NIC that was applied ($R_N = -20$ MΩ, and $R_N = -4$ kΩ, respectively) and for low, medium, and high error amplifier gain ($K = 10$, $K = 100$, and $K = 1000$, respectively). In Fig. 8, there are limits on the residual phase error. As expected, the residual error gets smaller as the control loop gain rises. The loop gain is dependent not only on the amplifier gain but also on the phase detector sensitivity, which is proportional to the voltage across the tank. This voltage decreases due to increased damping by eddy currents as the probe gets closer to the target, resulting in a decrease in the loop gain. These effects contribute to the rise of a residual phase error for decreasing displacement, but for even smaller displacement, the error decreases after peaking. As the displacement gets even smaller, the tank quality factor Q_T becomes very small due to heavy damping by the eddy currents. This instance results in a smaller phase error for the same *frequency detuning* δ_ω as the steepness of the tank phase characteristic decreases for small Q_T. Based on Fig. 8, it is apparent that the residual phase error is prohibitively high

$$\varphi(d) + \varphi_0 = -\arctan\left\{-\frac{Q_p(d)}{1 + \frac{C_P}{C_{VB}}} \cdot \left[\frac{1}{\left[1 + \frac{K}{V_B - \Phi} \cdot \left[V_{\rm os} - \frac{V_i(d)}{\pi} \cdot \sin\varphi\right]\right]^n} - 1\right]\right\} \qquad (14)$$

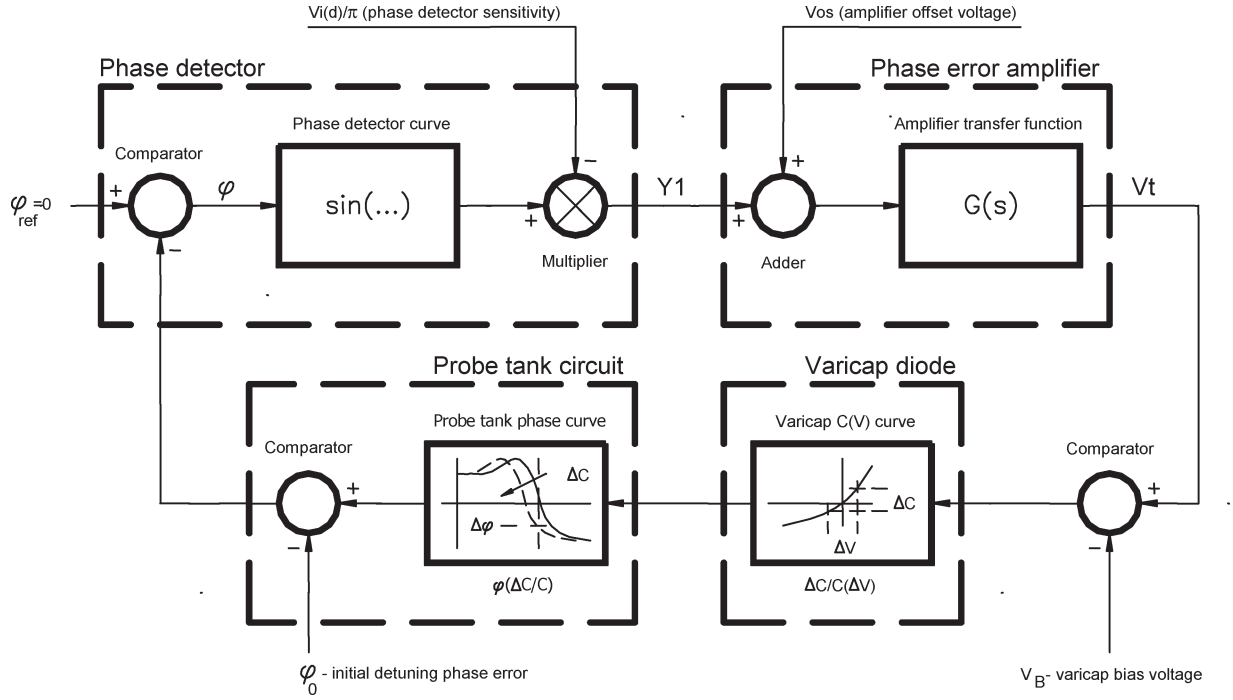

Fig. 7. Resonance control-loop model.

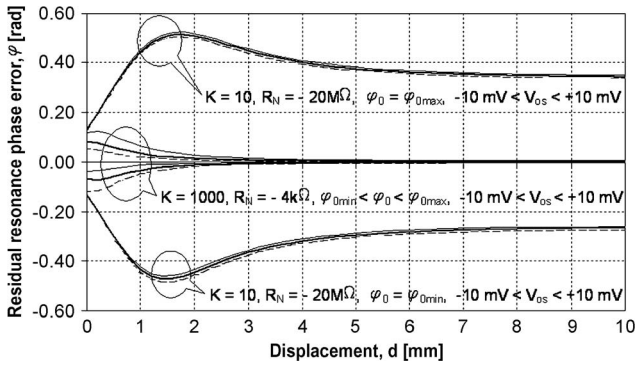

Fig. 8. Residual phase-error limits bounded by the amplifier gain and negative conductance applied at the input.

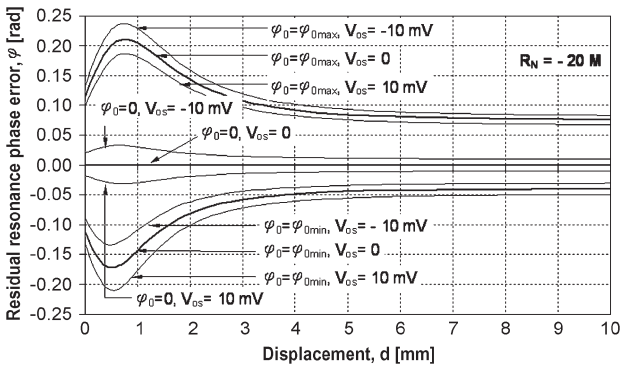

Fig. 9. Residual phase error for almost no negative conductance applied at the input ($R_N = -20$ MΩ) and a medium error amplifier gain ($K = 100$).

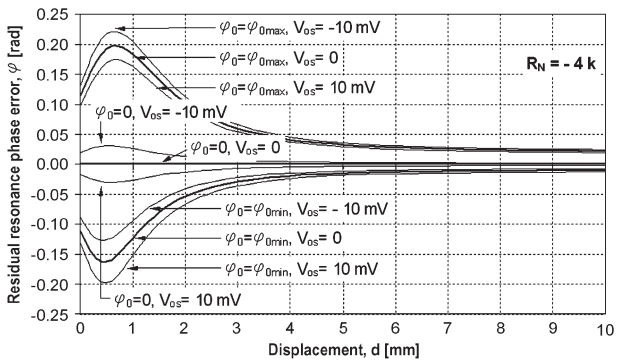

Fig. 10. Residual phase error for maximum negative conductance applied at the input ($R_N = -4$ kΩ) and a medium error amplifier gain ($K = 100$).

for a low amplifier gain ($K = 10$) and the minimum negative conductance applied ($R_N = -20$ MΩ), but it is almost negligible for a high gain ($K = 1000$) and the maximum negative conductance ($R_N = -4$ kΩ). Although the very high amplifier gain would best suit the phase-error constraint, the amplifier upper frequency limit should also be addressed. Depending on the transducer application, the resonance control-loop response should accordingly be tailored. For instance, if the transducer will be used for the monitoring vibration of the high-speed gas turbine, the measurement bandwidth should extend to at least several kilohertz. Then, the resonance control-loop bandwidth should be at least ten times wider, extending to at least 10 kHz. The amplifier with a closed-loop gain of 60 dB ($K = 1000$) and a bandwidth of more than 10 kHz is just the limit that can be achieved with standard operational amplifiers. It would be worth exploring if the moderate amplifier gain ($K = 100$) would be sufficient for somewhat greater but still acceptable residual phase error. In Figs. 9 and 10, there are residual phase-error details for a medium amplifier gain. The error peaks to approximately 0.2 rad at a rather small displacement of 0.5 mm, which can be considered the lower edge of the transducer operating range. For a large displacement, the error drops below 0.1 rad, even for small negative conductance applied. For more negative conductance applied, the error is even smaller. The

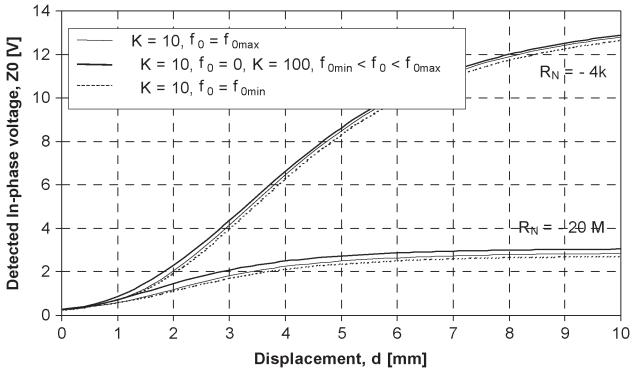

Fig. 11. Effect of residual phase error on the transducer transfer curve.

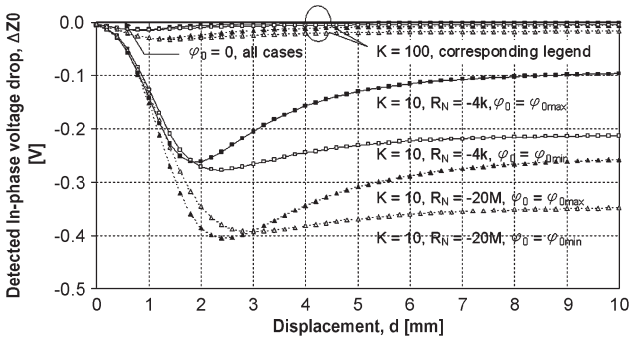

Fig. 12. Deviation of the transducer transfer curve from the curve for ideal resonance tuning.

effect of residual phase error on the transducer transfer curve is shown in Figs. 11 and 12. The effect of residual phase error on the transducer transfer curve is observable for a low error amplifier gain ($K = 10$), whereas for a medium gain ($K = 100$), it is negligible. This result proves the assumption that the gain of 40 dB would be sufficient right, making the tradeoff between the gain and the bandwidth easier. Fig. 12 shows the deviation of the transducer transfer curve from the curve with ideal resonance tuning, e.g., zero residual phase error.

VI. NIC

There have been many NIC circuits introduced, but none of them possesses the possibility of easy adjustment by either dc voltage or current controlled by a potentiometer or, in the case of series production, generated by a digital/analog converter (DAC). This condition is important if the transducer will digitally be calibrated with the adjustment and calibration data stored in the transducer electronic data sheet. The new voltage-controlled NIC circuit is presented in Fig. 13. Based on Fig. 13, the ac dynamic current through Z is proportional to the V/Z ratio (presuming that the $V_{\rm BE}$ of transistors Q_5 and Q_6, as well as the biasing sources $V_{\rm B}$ and $I_{\rm B}$, are constant). This current flows into the emitters of Q_5 and Q_6 and eventually develops the collector currents of Q_5 and Q_6. Transistor pairs Q_1–Q_2 and Q_3–Q_4 steer the Q_5 and Q_6 collector currents into the NIC input currents I_{01} and I_{02}. Distribution of the Q_5 and Q_6 collector currents between I_{01} and I_{02} is controlled by the control voltage $V_{\rm c}$. If one of the input ports is grounded, the corresponding input current is sunk into the ground, whereas the

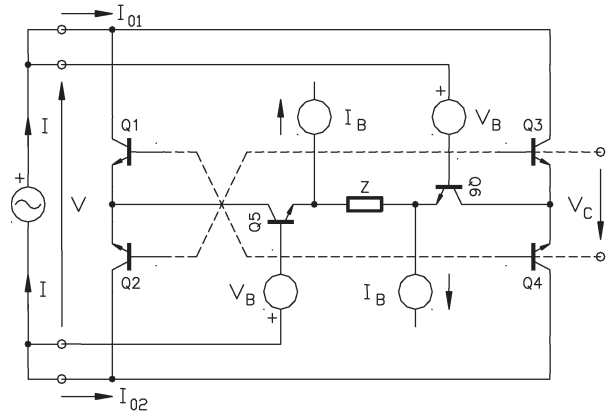

Fig. 13. Voltage-controlled NIC circuit.

other input current loads the signal voltage source V connected to the input. The loading current is proportional to V/Z; thus, the whole circuit loads the signal source with an impedance proportional to Z. The factor of proportionality depends on the level and polarity of $V_{\rm c}$, and the input admittance of the circuit can be varied in the range $-1/Z$ to $1/Z$. The circuit can be adjusted either as a positive impedance converter (e.g., positive loading impedance) or as an NIC.

A. NIC Input Admittance

With respect to Fig. 13, the following relations hold:

$$I_Z = -\frac{V-(V_{BE6}-V_{BE5})}{Z} \tag{16}$$

$$I_{E1} = \frac{I_{C5}}{1+e^{-\frac{V_c}{V_T}}} \quad I_{E2} = \frac{I_{C5}}{1+e^{\frac{V_c}{V_T}}} \tag{17}$$

$$I_{E3} = \frac{I_{C6}}{1+e^{\frac{V_c}{V_T}}} \quad I_{E4} = \frac{I_{C6}}{1+e^{-\frac{V_c}{V_T}}} \tag{18}$$

$$I_{C5} = \alpha_5 \cdot I_{E5} = \alpha_5 \cdot (I_Z + I_B) \tag{19}$$

$$I_{C6} = \alpha_6 \cdot I_{E6} = \alpha_6 \cdot (-I_Z + I_B) \tag{20}$$

$$I_{01} = I_{C1} + I_{C3} \quad I_{02} = I_{C2} + I_{C4} \tag{21}$$

where the base currents of Q_5 and Q_6 are neglected, $V_T = (k \cdot T/q)$ is the voltage equivalent of absolute temperature T, k is the Boltzman constant, q is the elementary electric charge, α is the transistor common-base current gain, $V_{\rm BE}$ is the transistor base to emitter voltage, I_C is the transistor collector current, and I_E is the transistor emitter current. Numeric indices correspond to particular transistors in Fig. 13; for instance, I_{E1} is the emitter current of Q_1. Combining (16)–(21), the expressions for the NIC input currents result in (22) and (23). Differentiating (22) and (23) with respect to V, the NIC dynamic input admittance follows (24) and (25). In this process, one of the NIC ports is assumed to be grounded, and differentiation is performed on the other port current with respect to V. For instance, while deriving Y_{01}, port 2 is grounded, and I_{02} flows into the ground, and while deriving Y_{02}, port 1 is grounded, and I_{01} flows into the ground.

Assuming the matched transistors in the circuit (which is plausible if the integrated circuit realization of the NIC is presumed), (24) and (25) can further be simplified by

approximation, i.e.,

$$\alpha_1 \approx \alpha_2 \approx \alpha_3 \approx \alpha_4 \approx \alpha_5 \approx \alpha_6 \approx \alpha$$

$$I_{01} = \frac{\alpha_1 \cdot \alpha_5 \cdot \left(1 + e^{\frac{V_c}{V_T}}\right) - \alpha_3 \cdot \alpha_6 \cdot \left(1 + e^{-\frac{V_c}{V_T}}\right)}{\left(1 + e^{-\frac{V_c}{V_T}}\right) \cdot \left(1 + e^{\frac{V_c}{V_T}}\right)} \cdot I_Z + \frac{\alpha_1 \cdot \alpha_5 \cdot \left(1 + e^{\frac{V_c}{V_T}}\right) + \alpha_3 \cdot \alpha_6 \cdot \left(1 + e^{-\frac{V_c}{V_T}}\right)}{\left(1 + e^{-\frac{V_c}{V_T}}\right) \cdot \left(1 + e^{\frac{V_c}{V_T}}\right)} \cdot I_B \tag{22}$$

$$I_{02} = \frac{\alpha_2 \cdot \alpha_5 \cdot \left(1 + e^{-\frac{V_c}{V_T}}\right) - \alpha_4 \cdot \alpha_6 \cdot \left(1 + e^{\frac{V_c}{V_T}}\right)}{\left(1 + e^{-\frac{V_c}{V_T}}\right) \cdot \left(1 + e^{\frac{V_c}{V_T}}\right)} \cdot I_Z + \frac{\alpha_2 \cdot \alpha_5 \cdot \left(1 + e^{-\frac{V_c}{V_T}}\right) + \alpha_4 \cdot \alpha_6 \cdot \left(1 + e^{\frac{V_c}{V_T}}\right)}{\left(1 + e^{-\frac{V_c}{V_T}}\right) \cdot \left(1 + e^{\frac{V_c}{V_T}}\right)} \cdot I_B \tag{23}$$

$$Y_{01} = \frac{dI_{01}}{dV} = \frac{\alpha_1 \cdot \alpha_5 \cdot \left(1 + e^{\frac{V_c}{V_T}}\right) - \alpha_3 \cdot \alpha_6 \cdot \left(1 + e^{-\frac{V_c}{V_T}}\right)}{\left(1 + e^{-\frac{V_c}{V_T}}\right) \cdot \left(1 + e^{\frac{V_c}{V_T}}\right)} \cdot \left(-\frac{1}{Z}\right) \tag{24}$$

$$Y_{02} = \frac{dI_{02}}{dV} = \frac{\alpha_2 \cdot \alpha_5 \cdot \left(1 + e^{-\frac{V_c}{V_T}}\right) - \alpha_4 \cdot \alpha_6 \cdot \left(1 + e^{\frac{V_c}{V_T}}\right)}{\left(1 + e^{-\frac{V_c}{V_T}}\right) \cdot \left(1 + e^{\frac{V_c}{V_T}}\right)} \cdot \left(-\frac{1}{Z}\right) \tag{25}$$

$$Y_{01} \approx \alpha^2 \cdot \frac{e^{\frac{V_c}{V_T}} - 1}{e^{\frac{V_c}{V_T}} + 1} \cdot \left(-\frac{1}{Z}\right) \tag{26}$$

$$Y_{02} \approx -\alpha^2 \cdot \frac{e^{\frac{V_c}{V_T}} - 1}{e^{\frac{V_c}{V_T}} + 1} \cdot \left(-\frac{1}{Z}\right). \tag{27}$$

Based on (26) and (27), it is apparent that the NIC input admittance is voltage controlled by V_c and can be adjusted in the range $1/Z$ to $-1/Z$, depending on the value and polarity of V_c. The Y_{01} control curve is shown in Fig. 14. It is nonlinear and temperature dependent due to the temperature dependence of V_T. The Y_{02} curve is the mirror image of Y_{01} mirrored around the V_c axis (see Fig. 14).

B. NIC Temperature Compensation

In the first approximation, (26) and (27) are temperature dependent mainly due to the temperature-dependent argument of the exponential function. However, this argument is not the only temperature-dependent factor. Transistor common-base current gain is dependent not only on temperature but also on the transistor collector current that might also be temperature dependent by design. Therefore, Y_{01} or Y_{02} is a complex function of temperature. To derive this function, α is first expressed in terms of β, the transistor common-emitter current gain that is usually cited in transistor's data sheet, where $\alpha = \beta/(1+\beta)$. Substituting it for α in (26) or (27) and differentiating with respect to T, the input admittance sensitivity to temperature follows (28). In (28), there are factors that are technology dependent, e.g., $(\partial\beta/\beta)/\partial T$, which is the transistor common-emitter current gain dependence upon temperature, and $(\partial\beta/\beta)/\partial I_C$, which is the transistor common-emitter current gain dependence upon collector current, as well as factors that are design dependent, e.g., $(\partial I_C/I_C)/\partial T$ and $(\partial V_c/V_c)/\partial T$. These design-dependent factors give freedom of proper adjustment for temperature compensation of the NIC input admittance. The transistor β rises (1–2)%/°C for most transistors and by some 10%/mA of collector current. The temperature sensitivity of β is much more uniform than the collector current sensitivity, which much more varies with transistor types. We have

$$\frac{\frac{\partial Y_{01}}{Y_{01}}}{\partial T} = \frac{2}{1+\beta} \cdot \left\{ \left[\frac{\left(\frac{\partial\beta}{\beta}\right)}{\partial T} \right] + I_C \cdot \left[\frac{\left(\frac{\partial\beta}{\beta}\right)}{\partial I_C} \right] \cdot \frac{\frac{\partial I_C}{I_C}}{\partial T} \right\} + \frac{2 \cdot \frac{V_c}{V_T} \cdot e^{\frac{V_c}{V_T}}}{e^{2 \cdot \frac{V_c}{V_T}} - 1} \cdot \left(\frac{\frac{\partial V_c}{V_c}}{\partial T} - \frac{1}{T} \right). \tag{28}$$

For this reason, the transistor collector currents, e.g., bias current I_B in the design of the transducer is maintained constant, which is supplied by the temperature stable current source. The remaining positive temperature dependence, e.g., $(\partial\beta/\beta)/\partial T$, can be compensated by $[(\partial V_c/V_c)/\partial T - 1/T]$ properly

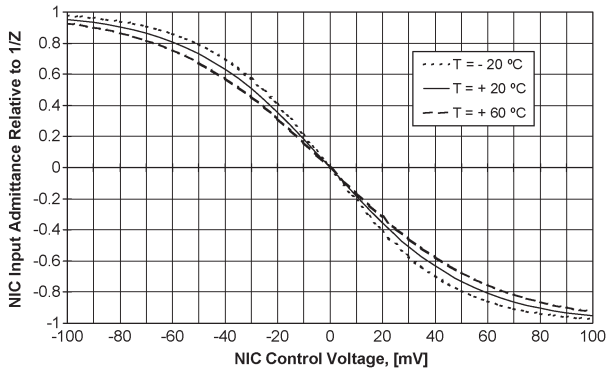

Fig. 14. NIC input admittance Y_{01} normalized to $1/Z$ relative to the NIC control voltage V_c.

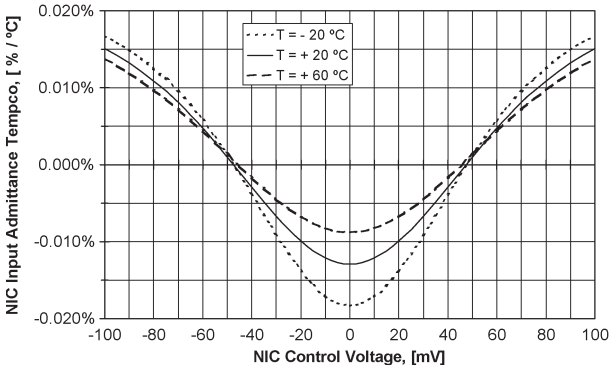

Fig. 15. Optimized NIC input admittance temperature coefficient relative to the NIC control voltage V_c.

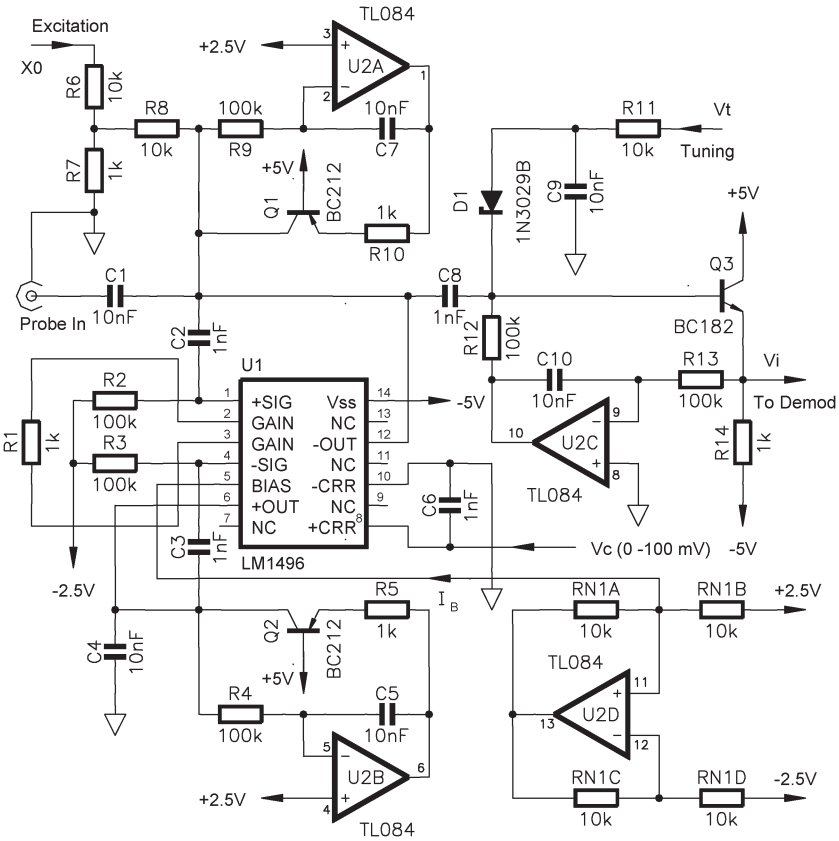

Fig. 16. Input section of the prototype eddy-current displacement transducer.

adjusted to adequate negative value. It requires the NIC control voltage V_c to be generated from the temperature-dependent reference voltage, with the positive temperature coefficient (tempco) somewhat smaller than $1/T$. Assuming an average transistor current gain $\beta \approx 100$, the $(\partial V_c/V_c)/\partial T = c \cdot (1/T)$, with $0.85 \leq c \leq 0.95$, would best compensate for the overall NIC tempco for $(\partial\beta/\beta)/\partial T$ in the range (1–2)}%/°C. The resulting NIC tempco for $c = 0.9$ is shown in Fig. 15. The resulting tempco is very small for V_c equal to approximately $\pm$50 mV. By careful selection of Z, which would require fine adjustment of V_c around 50 mV, the NIC input admittance could be made virtually temperature independent. The temperature-stable NIC input admittance would then fully comply with the transducer stability constraints. Allowing nonideal temperature compensation that leads to the NIC input admittance tempco constrained to $\pm 0.01\%/°\text{C}$, the transducer tempco $S_T^{|Z(d)|_{\text{res}}}$ would then, in the worst case, be limited to

$$S_T^{|Z(d)|_{\text{res}}} = S_{R_N}^{|Z(d)|_{\text{res}}} \cdot S_T^{R_N} = (-3) \cdot (\pm 0.01\%/°\text{C}) = \pm 0.03\%/°\text{C}$$

with the sensitivity to R_N, $S_{R_N}^{|Z(d)|_{\text{res}}}$ being bound to -3 (see Fig. 5).

VII. Transducer Input Section

The NIC structure in Fig. 13 can be identified in the circuit of the standard commercially available integrated balanced modulator/demodulator circuit LM1496. The input section of the prototype transducer was therefore designed around LM1496 and is presented in Fig. 16. U_1 is configured as the NIC in Fig. 13. Resistor R_1 corresponds to Z. For the best performance, it should be a stable high-precision metal-film resistor. The rest of the components around U_1 are not critical. U_{2A}, U_{2B}, Q_1, Q_2, and the passive components that are correspondingly connected are used for proper biasing of U_1. Q_3 is the probe signal buffer, where U_{2C} is used for Q_3 emitter biasing at zero volts to remove any dc offset from V_i that could compromise the detection process. U_{2D} and resistors R_{N1A}, R_{N1B}, R_{N1C}, and R_{N1D} constitute the constant current source of 0.5 mA for the biasing collector currents of transistors in U_1 (e.g., I_B in Fig. 13). The nice touch is the use of the Zener diode 1N3029B (D_1). It is reverse biased but is always below its breakdown voltage (24 V). The bias is controlled by the tuning control voltage V_t. The diode exhibits considerable capacitance (100–500 pF) that is varied by V_t; thus, it is used as a varicap. The commercial varicap diodes with the capacitance in that range are otherwise not easy to find.

VIII. Reference-Signal Generator

The reference signals for in-phase and quadrature detection are square-wave signals X_0 and X_1 [1]. X_1 lags behind X_0 by a quarter period $(\pi/2)$. The frequency of X_0 and X_1 is stable to avoid the variable probe excitation frequency that would affect the transducer sensitivity due to a change in the eddy-current losses in the target with varying frequency, e.g., creating the phony displacement signal. The reference generator

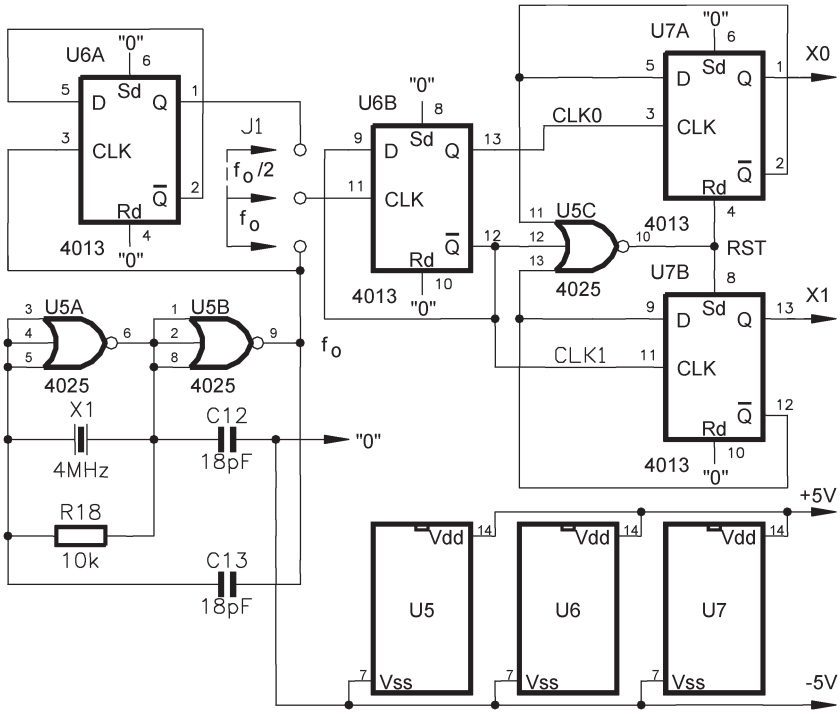

Fig. 17. Reference generator of the prototype eddy-current displacement transducer.

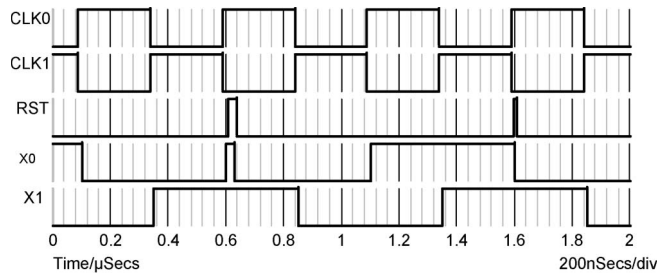

Fig. 18. Waveforms of the prototype eddy-current displacement transducer reference-signal generator.

circuit is shown in Fig. 17. U_{5A} and U_{5B} create the clock generator. The clock frequency is crystal controlled by X_1. If less accuracy is sufficient, X_1 could simply be omitted, and the frequency will be determined by R_{18}, C_{12}, and C_{13}. All of the D flip-flops are wired in a "divide by 2" configuration, e.g., the frequency at their Q outputs is half the frequency at their CLK inputs. U_{6A} is simply used as the clock frequency divider by 2 if it would be necessary to select the lower operating frequency by reposition of the jumper J_1. U_{5C} is used to generate the proper reset signal to flip-flops U_{7A} and U_{7B}. Without this provision, U_{7A} and U_{7B} initial setup would be random at powerup, leading to a possibly wrong sequence, e.g., X_0 lags behind X_1 and not vice versa. The waveforms of the reference generator are shown in Fig. 18, emphasizing the correct signal sequence.

IX. NIC Control Voltage Generator

In Section VI, it was established that the NIC control voltage should be variable in the range 0–100 mV with a tempco of approximately $0.9 \cdot 1/T$. The p-n junction exhibits a tempco of $-1/T$. To achieve the required tempco, it is needed to invert it and attenuate by some 10%.

Attenuation could be achieved by adding some temperature-stable voltage to the temperature-dependent voltage with a tempco of $1/T$. The control voltage generator based on this idea is shown in Fig. 19. The voltage reference REF02 (U_3) is used with U_{4B}, R_{N2A}, R_{N2C}, R_{N2E}, and R_{N2G} to create the symmetric temperature stable reference voltages $\pm$ 2.5 V. The REF02 Temp output voltage equals 630 mV (p-n junction forward voltage) referenced to -2.5 V but with a tempco of $+1/T$. Some temperature-stable voltage adjusted with R_{16} that is added to it was derived from the $\pm$ 2.5V supplies. The resulting voltage with proper tempco is attenuated by R_{17}, driving the difference amplifier to comprise U_{4C}, R_{N3C}, R_{N3D}, R_{N3E}, and R_{N3F}. The U_{4C} output voltage is the required V_c referenced to ground, adjustable in the range 0–100 mV, with the right tempco.

X. Demodulator Section

As described in Section I, the transducer demodulation section is designed as the set of in-phase and quadrature synchronous demodulators. In contrast to widely used peak detectors for this purpose, the synchronous demodulation provides for averaging that can be very useful for the suppression of spikelike interference signals that might arise from the residual magnetism in the observed target (the standard problem in monitoring rotational machinery). Synchronous detection is performed with simple switches and RC averaging of the switch output voltages. The demodulator section circuits are shown in Fig. 20. Switches U_{8A} and U_{8D} comprise the in-phase detector, whereas

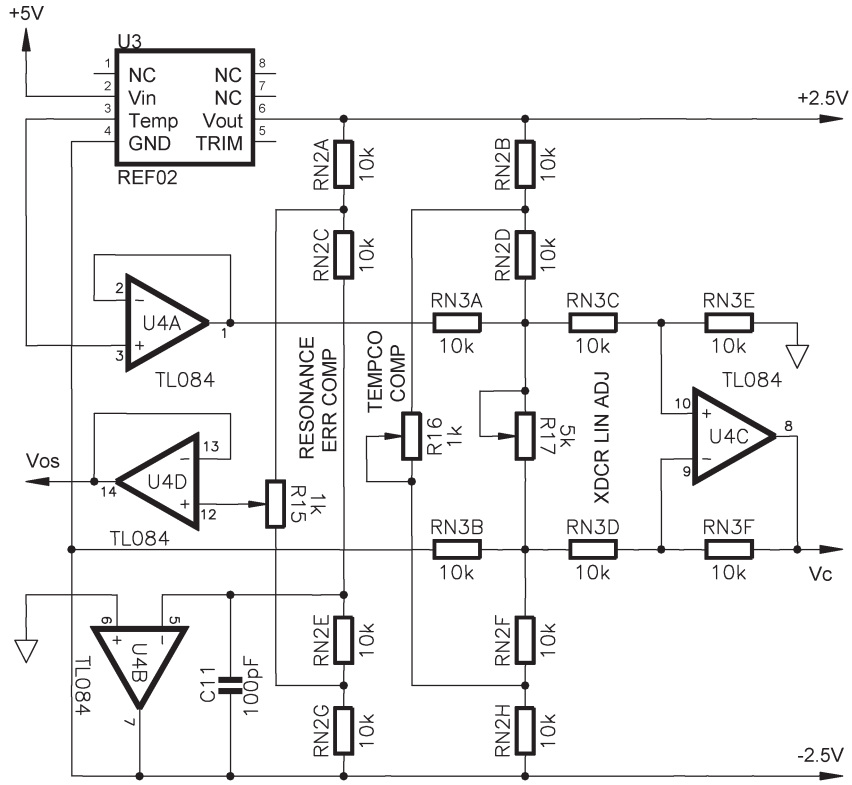

Fig. 19. Prototype eddy-current displacement transducer NIC control voltage generator.

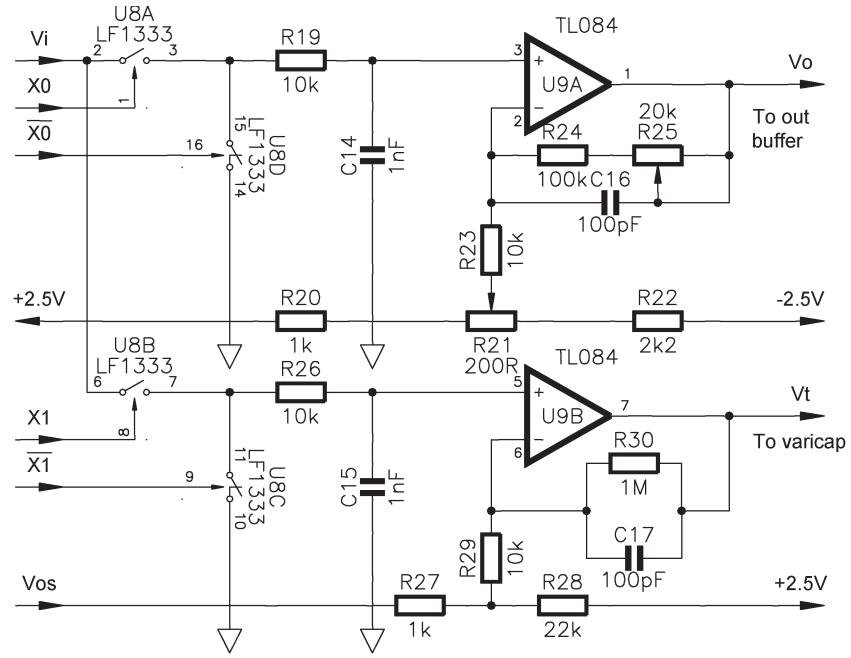

Fig. 20. Prototype eddy-current displacement transducer demodulator section.

switches U_{8B} and U_{8C} comprise the quadrature detector. Low-pass filtration (averaging) is accomplished by simple RC low-pass filters made of R_{19}/C_{14} and R_{26}/C_{15}, respectively. U_{9A} and U_{9B} are the output amplifier and the phase-error amplifier, respectively. The transducer sensitivity is fine adjusted by R_{25}, whereas the output offset is fine adjusted by R_{21}. $V_{\rm os}$ that was generated in the NIC control voltage generator compensates for the resonance tuning error due to the U_{9B} offset.

XI. Measurement Results

The prototype transducer was assembled according to the design details in Figs. 16–20. After optimization of adjustments with R_{17} (linearity), R_{15} (residual resonance error), R_{21} (output offset), and R_{25} (sensitivity), the transducer transfer curve was obtained as shown in Fig. 21. The NIC control voltage was adjusted to 27.5 mV, which is somewhat less than the value for ideal tempco compensation ($\sim$50 mV). Further careful

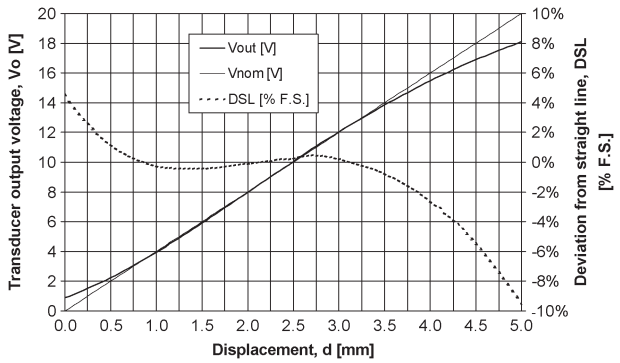

Fig. 21. Prototype eddy-current displacement transducer optimized transfer curve.

selection of R_1 (see Fig. 16) could move the optimal NIC control voltage to approximately 50 mV, which would result in near-ideal temperature compensation. Based on Fig. 21, it is apparent that the transducer linear range extends from 0.25 to 3.75 mm with a probe diameter of 8 mm [1], [2] while maintaining nonlinearity contained within $\pm 2\%$ F.S. The industry standard transducer with the same probe diameter and nonlinearity [12] has a linear range of 80 mils (2 mm). The achieved improvement is at least 60% without postdetection linearization. It could further be improved with postlinearization. The transducer tempco was not exactly measured due to the unavailability of the temperature chamber. However, some rough tests were performed by local heating of LM1496 and REF02. The compensating effect was observed as the heating of LM1496 lowered the output voltage, whereas heating of REF02 increased it.

XII. Conclusion

Design constraints of the eddy-current displacement transducer have carefully been analyzed. It has been proven that application of the negative conductance at the transducer input can compensate for the intrinsic probe losses that mask the eddy-current damping at large displacement [1], [2]. That way, the resonance impedance inversion method of transducer linearization [1] is made feasible, liberating the transducer circuit of post linearization. The transducer linear range is, by the application of the negative conductance, expected to be almost doubled compared to results achieved by various authors using other methods [4]–[9]. It is emphasized that the proper resonance tuning is essential for the method to be effective. The residual resonance tuning error is governed by the performance of the resonance control loop. The nonlinear loop equation was solved for various parameter values that affect it. The phase-error amplifier gain is indicated as the main constraint for the resonance tuning quality. It has been proven that a moderate gain of 40 dB is sufficient, making deviation of the transducer transfer curve from the curve for ideal resonance tuning negligible while, at the same time, providing adequate loop bandwidth for typical transducer applications (e.g., vibration monitoring). The prototype eddy-current displacement transducer has been designed according to the design constraints that were developed. The most critical detail, e.g., the new NIC, has been designed with a topology that corresponds to the industry standard integrated circuit LM1496. The achieved temperature stability of the transducer is excellent. The displacement probe losses compensation by the NIC negative conductance and the automatic tuning into resonance resulted in the extension of the transducer linear range, which now covers a range of 0.25–3.75 mm (3.5 mm), approximately 44% of the probe diameter (8 mm), which is, at least, a 75% improvement to the best standard industrial grade commercially available transducer (80 mil $\sim$2 mm) [12]. Further extension of the linear range can be achieved by postdetection linearization. The transducer can easily be integrated in the IC form if the serial production would be decided upon.

References

[1] D. Vyroubal and D. Zele, "Experimental optimization of the probe for eddy-current displacement transducer," *IEEE Trans. Instrum. Meas.*, vol. 42, no. 6, pp. 995–1000, Dec. 1993.

[2] D. Vyroubal, "Impedance of the eddy-current displacement probe: The transformer model," *IEEE Trans. Instrum. Meas.*, vol. 53, no. 2, pp. 384–391, Apr. 2004.

[3] M. H. Norwwod and E. Shatz, "Voltage variable capacitor tuning: A review," *Proc. IEEE*, vol. 56, no. 5, pp. 788–798, May 1968.

[4] G. A. Girgis, K. Horn, and G. Kruse, "Measurement of mechanical vibration using eddy current transducers and simple digital demodulation techniques," *IEEE Trans. Instrum. Meas.*, vol. 35, no. 1, pp. 135–140, Feb. 1988.

[5] K. D. Anim-Appiah and S. M. Riad, "Analysis and design of ferrite cores for eddy-current-killed oscillator inductive proximity sensors," *IEEE Trans. Magn.*, vol. 33, no. 3, pp. 2274–2281, May 1997.

[6] Q. Li and F. Ding, "Novel displacement eddy-current sensor with temperature compensation for electrohydraulic valves," *Sens. Actuators A, Phys.*, vol. 122, no. 1, pp. 83–87, Jul. 2005.

[7] D. J. Sadler and C. H. Ahn, "On-chip eddy-current sensor for proximity sensing and crack detection," *Sens. Actuators A, Phys.*, vol. 91, no. 3, pp. 340–345, Jul. 2001.

[8] P. Arpaia, P. Daponte, D. Grimaldi, and L. Michaeli, "ANN-based error reduction for experimentally modeled sensors," *IEEE Trans. Instrum. Meas.*, vol. 51, no. 1, pp. 23–30, Feb. 2002.

[9] T. Mizuno, S. Enoki, T. Hayashi, T. Asahina, and H. Shinagawa, "Extending the linearity range of eddy-current displacement sensor with magnetoplated wire," *IEEE Trans. Magn.*, vol. 43, no. 2, pp. 543–548, Feb. 2007.

[10] M. Jagiella, S. Fericean, and A. Dorneich, "Progress and recent realizations of miniaturized inductive proximity sensors for automation," *IEEE Sensors J.*, vol. 6, no. 6, pp. 1734–1741, Dec. 2006.

[11] S. Fericean and R. Droxler, "New nonconducting inductive analog proximity and inductive linear displacement sensors for industrial automation," *IEEE Sensors J.*, vol. 7, no. 11, pp. 1538–1545, Nov. 2007.

[12] Bently-Nevada, *Proximity Transducer Data Sheet.* [Online]. Available: www.gepower.com/prod_serv/products/oc/en/bently_nevada/sensor_trans.htm

Darko Vyroubal (M'95) was born in Karlovac, Croatia, in 1948. He received the B.Sc., M.Sc., and Ph.D. degrees in electronic engineering, with a major in electronic instrumentation and measurement, from the University of Zagreb, Zagreb, Croatia, in 1970, 1974, and 1985, respectively.

From 1970 to 1995, he was with the ENiN Institute, which is a subsidiary of the Jugoturbina Corporation, where he participated in the design and implementation of electronic instrumentation for diagnostics and monitoring of large machinery. From 1996 to 1998, he was with the ABB Power Plants Ltd., where he was involved in the design of automation systems for power plant control. Since 1998, he has been with the Polytechnic University of Karlovac, Karlovac, where he is currently a Full Professor and the Vice-Dean in charge of lecturing and research. He teaches electrical engineering, electronic measurement, and automatic control. He has published more than 30 papers. His research interests include electronic instrumentation and sensors.